

Solar Active Region Electric Currents Before and During Eruptive Flares

B. Schmieder¹ and G. Aulanier¹

LESIA, Observatoire de Paris, PSL Research University, CNRS, Sorbonne Universités, UPMC Univ. Paris 06, Univ. Paris Diderot, Sorbonne Paris Cité, 5 place Jules Janssen, F-92195 Meudon, France e-mail: brigitte.schmieder@obspm.fr

Received ...; accepted ...

ABSTRACT

Context. The chapter "Solar Active Region Electric Currents Before and During Eruptive Flares" is a discussion on electric currents in the pre-eruption state and in the course of eruptions of solar magnetic structures, using information from solar observations, nonlinear force-free field extrapolations relying on these observations, and three-dimensional magnetohydrodynamic (MHD) models. The discussion addresses the issue of neutralized vs. non-neutralized currents in active regions and concludes that MHD models are able to explain non-neutralized currents in active regions by the existence of strong magnetic shear along the polarity inversion lines, thus confirming previous observations that already contained this result. The models have also captured the essence of the behavior of electric currents in active regions during solar eruptions, predicting current-density increases and decreases inside flare ribbons and in the interior of expanding flux ropes respectively. The observed photospheric current density maps, inferred from vector magnetic field observations, exhibit similar whirling ribbon patterns to the MHD model results, that are interpreted as the signatures of flux ropes and of quasi-separatrix layers (QSLs) between the magnetic systems in active regions. Enhancement of the total current in these QSLs during the eruptions and decreasing current densities at the footpoint of erupting flux ropes, has been confirmed in the observations.

Aims.

Methods.

Results.

Conclusions.

Key words. Electric current in active regions and flares

1. INTRODUCTION

The occurrence of finite electric currents in the Sun's corona is a fundamental requirement for the existence of an active phenomena, such as solar flares and CMEs. Several reasons can be put forward. In the dilute corona, the plasma beta (β) is much lower than unity. So the structure of the coronal plasma is dominated by the magnetic field, and the magnetic energy is the main reservoir for all dynamics. Also, active phenomena occur on time-scales far shorter than those on which the dense photosphere evolves. So the distribution of magnetic flux crossing the photosphere hardly changes during solar transients. Given the solenoidal nature of the magnetic field, the potential (i.e. current-free) field corresponds to the lowest magnetic energy state for a fixed photospheric flux distribution. However, slow photospheric motions can induce twist and stress of the magnetic field lines and lead to a non potential magnetic field, which carries electric currents. So current-carrying magnetic fields constitute the source of energy for active phenomena. Also beyond this global property, electric currents play several key local roles in magnetohydrodynamics (MHD). The most significant examples are their presence in the Lorentz force, as well as in several terms of the generalized Ohm's law, including the usual resistive term and the Hall electric field which are both involved in magnetic reconnection within current sheets.

In spite of their importance, few studies have been realized on solar electric currents over several decades and up to very recently. The reason is probably theoretical, and observational.

Theoretically, several historical models had initially considered the electric current to be an input parameter. For example, "circuit models" for solar flares prescribed the total current I as it is in laboratory experiments (see e.g. Alfvén & Carlqvist 1967; Spicer 1982). More generally, one approach to plasma physics that is often used in the magnetospheric community (and is advocated by e.g. Melrose 1995; Heikkilä 1997) is to make every calculation with the equations that use the electric field \mathbf{E} and the current density \mathbf{J} as variables. This is the so-called " $\mathbf{E}; \mathbf{J}$ paradigm". But both circuit models and the $\mathbf{E}; \mathbf{J}$ paradigm have been criticized throughout the years (see Parker 1996a,b, 2001). In this line, E.N. Parker argued that they should be substituted by the " $\mathbf{B}; \mathbf{v}$ paradigm" in MHD. In the latter, the current densities \mathbf{J} merely result from the generation of a finite curl of the magnetic field \mathbf{B} through Ampère's equation, as a direct result of plasma flows \mathbf{v} through the ideal induction equation. So, the current is not a prime variable, since it does not even appear in the governing equations of MHD. For this reason, electric currents have been overlooked for years.

Observationally, the photospheric magnetic field vector in solar active regions provides the vertical component of curl \mathbf{B} . However the vector magnetic field can be measured only in the photosphere, and thus only the vertical component of the current density J_z passing through the photosphere to the corona can be identified. An idealized active region (AR) consists of two sunspots represented by a bipole with two opposite polarities linked by a flux tube (called a flux rope when it is twisted) in the corona. Since $\beta < 1$ in sunspots, the AR-scale magnetic-field

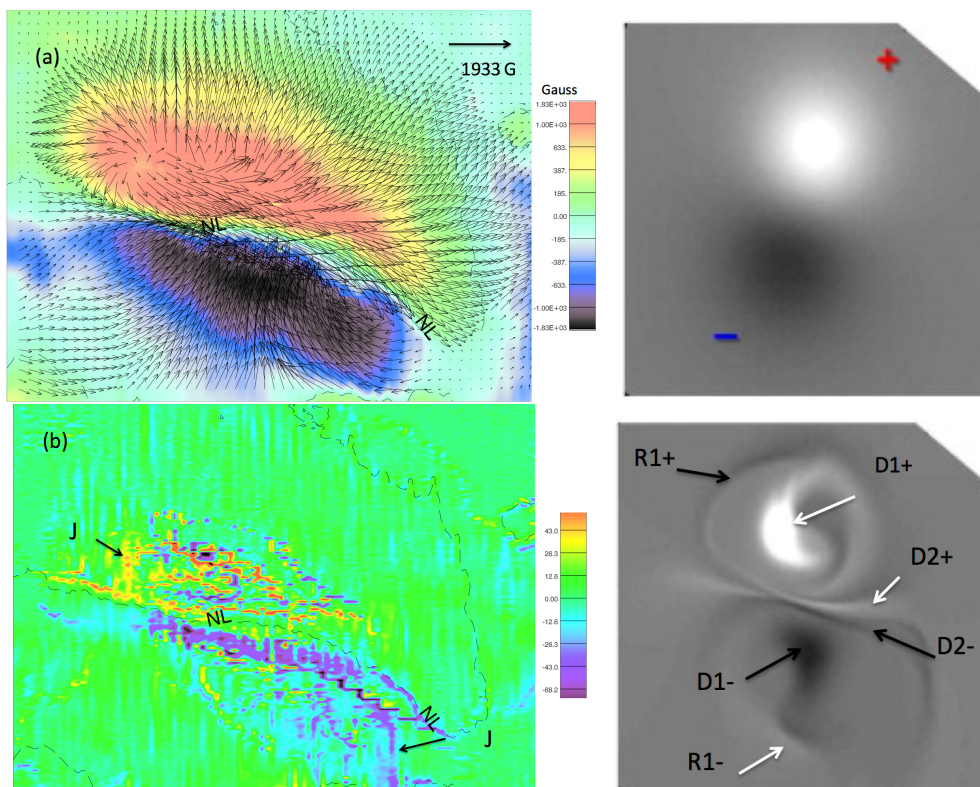


Fig. 1. Vector magnetogram and vertical component of the electric current density map in the emerging active region AR 10808 with positive helicity observed with the THEMIS vector magnetograph on September 13 2005 (Courtesy of Bommier). (a) B_z map with two elongated tongues symmetrical to the neutral line (NL or PIL) where the arrows represent the horizontal field (red-yellow represents the positive polarity, blue-violet the negative polarity between ± 1800 Gauss). (b) Vertical component of the electric current density in units of mA m^{-2} ; yellow represents the positive current while violet the negative current. The letters J and arrows point out the J-shaped current ribbons. (Right panels): Initial B_z in a bipole and vertical electric current density after applying a positive twist in the OHM simulation (adapted from Schmieder & Aulanier (2012), see Section 2.2). White areas correspond to positive B_z and J_z , dark-grey areas to negative B_z and J_z . D indicates direct currents, R return currents. Their sign is defined by the magnetic helicity convention shown in Table 1.

should be close to force free not only in the corona but also in the photosphere. Thus electric current density of both signs should be measured in sunspots indicating a flow of currents in both directions in the large scale coronal flux tube. Most (if not all) vector magnetic field measurements used are quite sparse as well as relatively unreliable outside sunspots and their close vicinity. So photospheric electric-current densities are rather difficult to measure using the transverse magnetic field, which was and still is, commonly very noisy. In past observations only one sign of electric current was detected in each polarity. A full neutralization of currents in an active region implies that the total net current is zero in each polarity of a bipole. Therefore, results such as net currents in active regions were regarded as uncertain (as reported by e.g. Gary et al. 1987; Hagyard 1988; Wilkinson et al. 1992; Leka et al. 1996; Leka & Skumanich 1999). With the development of new-generation and dedicated ground-based telescopes (e.g. THEMIS in Canary Islands) and space-borne (e.g. Hinode, *Solar Dynamic Observatory* SDO) missions, more complicated electric current patterns have been detected in each polarity of ARs.

Thus new MHD simulations have been developed during recent years. Some correspondence has been found with the observations. MHD simulations based on the existence of twisted flux ropes show that current densities of both signs exist. A twist of finite radius theoretically implies the occurrence of a sheath of currents at the edge of the twisted flux tube, which flows in an opposite direction to the direct currents. These are called the

return currents. A twisted flux tube of left-handed twist has a negative helicity and a direct electric current that flows anti-parallel to the magnetic field (and vice versa) (Démoulin 2007; Démoulin & Pariat 2009). The modern conventional definition in MHD simulations which holds for AR large-scale quasi force-free coronal-field is summarized in Table 1. Actually, this definition is consistent with the inference of direct current (i.e. with their dominant sign, as mentioned above) in past observations.

Indeed, observational studies by Wheatland (2000); Falconer et al. (2002); Ravindra et al. (2011); Georgoulis et al. (2012); Schmieder & Aulanier (2012) showed new and frequent evidences of net current in solar active regions. These relatively recent observations have revived the old debate from the "90s" about the neutralization, or not, of electric currents in active regions (Melrose 1991; Parker 1996a). In this perspective the MHD simulations developed by Török et al. (2014); Dalmasse et al. (2015) have explained how and why unneutralized current densities occur in active regions when magnetic shear is present along polarity inversion lines (PIL).

In parallel, progress on the description of the magnetic topology of active regions has contributed significantly to the interpretation of the current density patterns observed before and during eruptions. The field-aligned currents in line-tied force-free coronal structures, imply a direct continuity between the coronal and the photospheric currents, especially above sunspots where $\beta < 1$. Because of magnetic flux conservation along the flux tube, one can expect to see the footprint of the

Magnetic helicity	direct current	return current
$H_B > 0$	$J_Z B_Z > 0$	$J_Z B_Z < 0$
$H_B < 0$	$J_Z B_Z < 0$	$J_Z B_Z > 0$

Table 1. Electric current density signs for positive and negative magnetic helicity at active region scale.

coronal current densities in the photosphere. In other words, the photospheric current pattern in sunspots should show a cross-section of the electric current density distribution inside the flux tube. In addition to twisted flux tubes with their volume currents, other magnetic structures also exist in the corona and connect down to the photosphere. Among such structures, one can find open-closed boundaries that separate closed magnetic field above active regions from open field in their surroundings, and separatrices between different flux systems, or quasi-separatrix layers (QSLs), which are very narrow volumes across which field lines quickly change connectivity. In these thin volumes, electric current sheet can develop along their length and eventually trigger reconnection of the magnetic field lines, leading to flares (Démoulin et al. 1996a). Therefore during eruptions QSLs become very important structures. The footprints in the photosphere of these structures are thin lanes of QSLs, which appear as long and narrow hooks. These structures reveal the evolution of the electric current densities before and during eruptions, observationally and in MHD models (Janvier et al. 2014).

This chapter addresses some of these issues, and describes new publications with recent findings and interpretations resulting from coupling current measurements and MHD models. The next section is focused on the evidence of pre-eruption currents in active regions (Section 2), and the following section concerns the evolution of the currents during eruptions (Section 3). We conclude in Section 4.

2. PRE-ERUPTION CURRENTS IN ACTIVE REGION

2.1. Observations of Direct and Return Current

The photospheric current distribution is derived from measurements of the vector magnetic field using Ampère's law. The vector magnetic field is measured by using the Zeeman effect which is sensitive mainly in photospheric lines. Hence only the vertical component of electric current density J_z can be readily calculated in the photosphere. The first published calculations of J_z were presented by Severny (1964) and Moreton & Severny (1968) (see the thesis of Harvey 1969) and later by Hagyard (1988); Wilkinson et al. (1992), and Canfield et al. (1993). The J_z observations showed principally two areas of opposite sign electric current density partly overlying the leading and following polarities of active regions (AR). Electric currents in magnetically isolated regions flow from one polarity to the other polarity, and correspond to direct currents. This was the basis of flare models with unneutralized active regions.

Due to recent improvements in vector magnetographs the measurements of electric current density are more reliable and now direct and return electric currents are detectable. Recent measurements indicate commonly that the return currents in total are much smaller than the direct currents and a net current still exists. From recent observations using high spatial resolution vector magnetograms (*the Helioseismic and Magnetic Imager* HMI aboard SDO, *the Spectro Polarimeter* SP aboard Hinode) and ground based telescopes (e.g. THEMIS) active region current maps are routinely obtained. ARs with neutralized currents and ARs with unneutralized currents have been both ob-

served (Wheatland 2000; Metcalf et al. 2006; Ravindra et al. 2011; Georgoulis et al. 2012; Gosain et al. 2014; Schmieder et al. 2015; Cheng & Ding 2016; Zhao et al. 2016).

We select one example of an AR with electric current density observations obtained with THEMIS. From the retrieved Stokes parameters $IQUV$ of the vector magnetogram the three magnetic field components were obtained by using the Milne-Eddington inversion code UNNOFIT (Bommier et al. 2007). The active region was a new born active region (AR) (Li et al. 2007; Canou et al. 2009; Bommier 2013; Schmieder & Aulanier 2012; Schmieder et al. 2015). The photospheric magnetic field of the active region presented two elongated tongues of opposite polarities (Figure 1 a). The photospheric magnetic field vector direction (see the arrows in Figure 1a) suggests that the twist of the emerging flux tube is right handed i.e. has a positive helicity. It has been shown that such a tongue-shape pattern in the photospheric magnetograms indicates that the emergence of the flux tube is not completed (Chandra et al. 2009; Luoni et al. 2011). In fact, the tongue elongation pattern indicates the existence of an azimuthal component of the magnetic field around the axis of the Omega-shaped coronal flux tube, and therefore the sign of the twist of the emerging flux tube can be deduced (see Section 2.2). The current pattern shows J-shaped current ribbons (Figure 1b). The direct current occupies two J-shaped areas with two elongated lanes in the AR center along the PIL. The direct current density J_z has a positive sign over the positive magnetic polarity and vice versa according to the positive helicity of the active region (Table 1). At low resolution return currents are observed at the periphery of each sunspot as much weaker current densities and narrower current lanes. At high spatial resolution it should be still noted that the fibril nature of sunspot penumbrae there leads to mixed strong direct and return currents at small scale (Venkatakrishnan & Tiwari 2009). The observations of such return currents are at the limit of what can be identified on the edge of and away from sunspots because the photosphere is there far from force free, because at small scale the magnetic field is subject to granular motions. So we are only concentrating here on current in sunspots where B is sufficiently strong ($\beta < 1$).

These observations have been compared with theoretical results obtained by a MHD model created from a bipolar potential field by photospheric vortex flows using the OHM code (Aulanier et al. 2012) (see Section 2.3). The $\beta = 0$ simulation performed with the OHM code reproduced the evolution of an initially torus-unstable flux rope (Figure 1 right column).

The global pattern of the photospheric electric current density shows intense direct currents in the polarities surrounded by return currents with a J-shape, similar to the observations. The dominant direct current in the strong fields (encircled by hooks) are (D1+ and D1-). The hooks primarily have direct currents, surrounded by weaker return current densities (R1+ and R1-). D2+ and D2- are current density lanes in the central part of the active region.

The presence of these relatively narrow current density ribbons in the photosphere can be explained as follows. The connectivity domains are bordered by the quasi-separatrix layers (QSLs) where large magnetic field distortion could exist. Between the flux rope and the environment, coronal current density layers can be formed during the pre-eruptive phase. Along the QSLs, any small perturbation can induce an increase of the currents in these narrow layers which are rooted in the photosphere (Démoulin et al. 1996a). Therefore analyzing the electric current density maps in the photosphere can inform on the existence and the geometry of QSLs, and hence on the location of a flux rope. In particular, the hook-shape extremities of the current ribbons in

the current density maps are the signatures of the existence of a twisted flux rope. The curvature of the hook part of the J depends on the twist of the flux rope (Démoulin et al. 1996b). The review of Gibson et al. (2006) also provided the evolutionary picture accompanying the flux-rope formation with hook structures.

2.2. Current Neutralization in Active Regions: History

In the previous subsection we have reported on how observations, as well as one numerical simulation, showed the coexistence of direct and return currents at active region scales. Let us now discuss the issue of current neutralization, i.e. of when, how, and why, direct and current currents can become equal. Before describing the most recent joint observational and MHD results, we start by presenting an historical view of a long-lasting debate about whether or not a net current can exist in an active regions (Melrose 1991; Parker 1996a).

According to coronal models for solar flares (Sturrock & Stern 1980), the energy storage involves a non potential component of the magnetic field, which can be achieved by a twist or shear of the coronal magnetic field. Melrose (1991) proposed a *reductio ad absurdum* argument. As a first point in his discussion, he argued that in an idealized case, if the currents were generated by photospheric or sub-photospheric stresses after an isolated magnetic flux tube had emerged, then the currents (directed along the flux tube axis) should be neutralized. He pursued his reasoning by saying that if electric currents were neutralized in the corona (i.e. the sum of direct currents should equal the sum of return currents). In the case of isolated flux ropes each direct current should be surrounded by return current on each side of the polarity inversion line (PIL). In the case of coherent shear, two elongated lanes of opposite currents along each side of the PIL should be observed. It is interesting to see that he predicted correctly the shape of the current density pattern obtained more than a decade later by MHD simulations (see Figure 2e here and Figure 2 in Melrose (1991)). But he did not correctly predict the neutralization. The reason is that in his argument, he considered a cylindrical and vertical flux tube anchored in the photosphere which has emerged completely. Treating the legs of active-region scale coronal-flux rope as being cylindrical and orthogonal to the photosphere was an oversimplification. Indeed new MHD models show that these legs are inclined and partially emerged from the solar interior (Leake et al. 2013; Török et al. 2014; Dalmasse et al. 2015).

In a second point of his reasoning, Melrose argued that neutralized currents were not measured (see Hagyard (1988) and Section 2.3). With these observational considerations, Melrose (1991) concluded that his basic assumption of neutralization of currents should not be valid, and he declared that the currents are unneutralized. This was a good conclusion, however this raised the question about where do the currents close. Spicer (1982) proposed an idea in the frame of a flare model based on an electric circuit. In that case the electric circuit was closed in the photosphere by cross-field horizontal currents. Nevertheless, this was not the solution proposed by Melrose (1991), who proposed instead that the electric current should close under the solar surface, deep in the solar dynamo region. This idea allowed the reconciliation of the observational results from this time with the theoretical approach. But then, one problem was the occurrence of elongated paths of net/unneutralized currents in the Sun's interior. Such net currents implied the existence of non isolated flux tubes, with structured azimuthal fields existing around the current paths everywhere inside the Sun. The problem was that these properties contradicted intuitive high- β behavior that isolate in

principle sub-photospheric flux ropes from their non-neutralized environment.

Melrose's physical thinking of unneutralized currents was correct. But it was impossible to see the role of magnetic shear at the PIL with a cylindrical geometry, since PILs simply do not exist in such a geometry. Also the poor observations available at this time were not granted since their noise hardly allowed to measure return current densities, which could have been weaker than the direct current densities.

All these ideas were debated in a series of papers (e.g. Melrose (1995); Parker (1996a,b)). Instead, Parker (1996b) argued that the net current must be zero, but that, because of a failure to resolve magnetic fibril structure, measurements of the field would incorrectly infer a non-zero net current.

The lack of return current in the past observations was due either to the return current strength being below the threshold of the measurements, or to the low spatial resolution of the former vector magnetographs (Leka et al. 1996), or to artifacts (e.g. Faraday rotation) as suggested by Wilkinson et al. (1992). The MHD simulations now consider 3D Omega-shaped loops that have different properties than the cylindrical flux tubes that were considered in the "90s" for the discussion about electric currents.

Both modern observational and theoretical improvements now permit us to resolve some of the problems debated between Parker and Melrose (see next Section).

2.3. Current Neutralization in Active Regions: Recent MHD Models

In the eruptive flare models of torus-type, only a net current is involved (van Tend & Kuperus 1978; Molodenskii & Filippov 1987; Martens & Kuin 1989; Forbes & Isenberg 1991; Forbes & Priest 1995; Lin & Forbes 2000; Lin et al. 2001; Kliem & Török 2006). Forbes (2010) showed that if return currents were introduced, they could stop the MHD instability.

Since the Melrose and Parker discussions, many theoretical models and MHD simulations have been proposed for flares and CMEs (Fan & Gibson 2003, 2007; Fan 2010; Aulanier et al. 2010; Amari et al. 2003a,b, 2014; Inoue 2016).

The recent flare and CME MHD models have been based on two mechanisms: emergence of current-carrying magnetic flux tubes through the photosphere (Leka et al. 1996; Cheung & Isobe 2014) or shearing of coronal field by photospheric horizontal flows (Klimchuk & Sturrock 1992; Török & Kliem 2003; Aulanier et al. 2005, 2010).

The question of whether net currents exist or not have been the motivation for the development of recent MHD models, which were dedicated to this question (Török et al. 2014; Dalmasse et al. 2015). Let us discuss in particular these two sets of theoretical papers based on mechanisms of injection of stress in the corona.

Török & Kliem (2003) studied the stressing of coronal magnetic field by photospheric motions of a bipole and noticed that net currents develop if the vortices are *close* enough to the PIL. Later Török et al. (2014), and Dalmasse et al. (2015) used respectively the Lare3D code (Leake et al. 2013) and the Observationally-driven High-order scheme Magnetohydrodynamic code (OHM) (Aulanier et al. 2005) to quantify net currents and to explain why they exist. In the simulation of Török et al. (2014) a sub-photospheric magnetic flux rope containing neutralized current was considered (Figure 2a). In the case of emergence of a flux tube, it has been shown that the flux tube looks like an Omega loop, starts to flatten below the so-

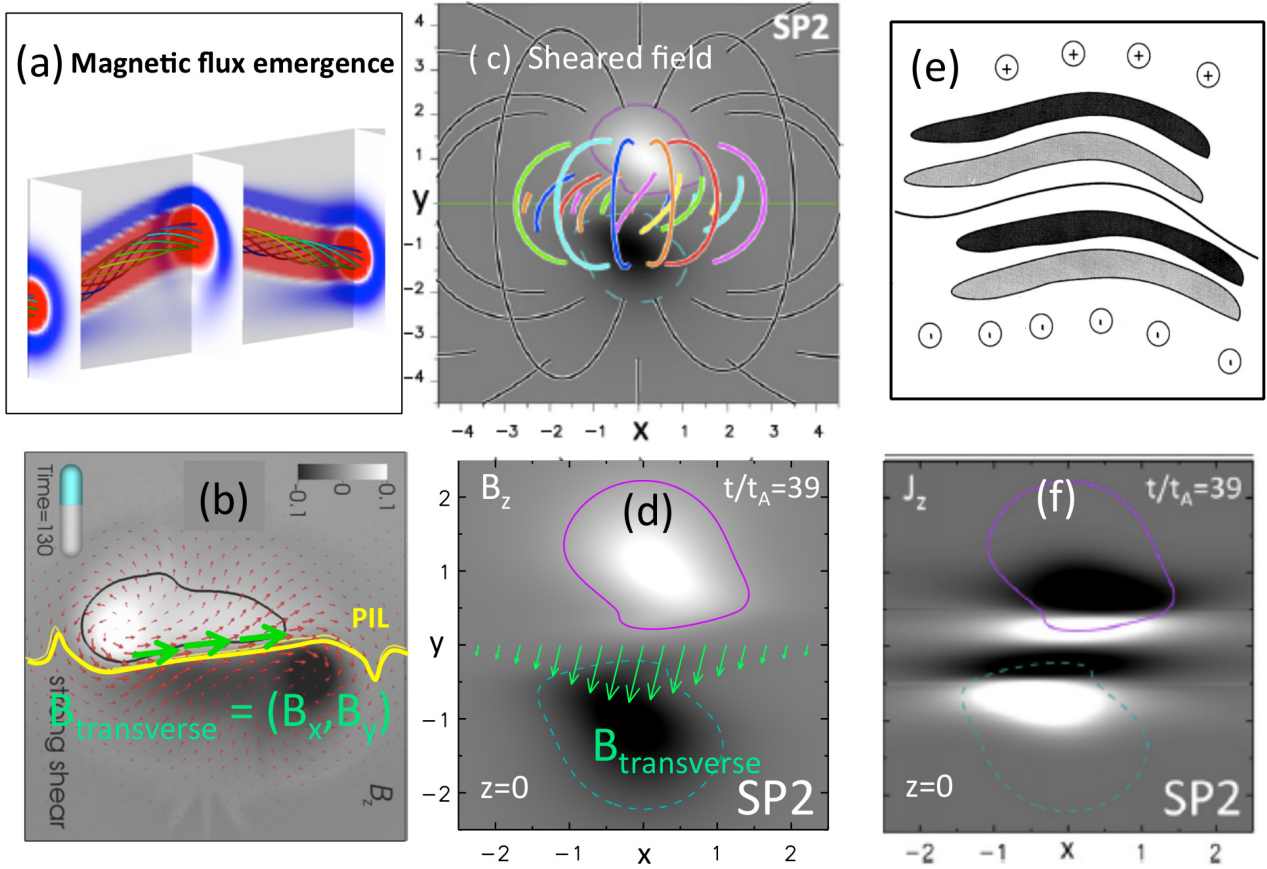


Fig. 2. MHD simulations of magnetic flux emergence. Panel (a) a model of emerging flux rope from Leake et al. (2013). Panels (b, c, d, f) results from the simulations of Dalmasse et al. (2015) showing in (b, c and d) the magnetic field B_z for different configurations of shear, the green arrows represent the transverse field between the two polarities. In Panel (f) the photospheric current density map J_z in the configuration shown in (c) and (d) with partially unneutralized currents to be compared with panel (e) showing the predicted sketch of Melrose (1991) for the idealized case of neutralization. Black areas display direct current and white areas return current on the positive polarity and the opposite on the negative polarity according to the negative sign of the helicity (left hand side twist) (see Table 1 and Section 2.2).

lar surface and emerges progressively (Archontis & Török 2008; Schmieder et al. 2014). Unneutralized (i.e. net) currents appear in the modeled photosphere when the flux tube has not completely emerged. The top part with direct currents has emerged while a non negligible part of return currents surrounding the flux tube is still below the photosphere.

Dalmasse et al. (2015) revisited the case of photospheric motions inducing stressed magnetic field by rotating and shearing the polarities of a bipole. In the case of twist, the photospheric vertical current density maps display direct and strong currents in the core of each polarity surrounded by a shell of return currents with a swirling pattern (see Figure 3 in Dalmasse et al. (2015)). This asymmetry is due to the effect of field line length resulting from the flux tube curvature. The stronger currents develop at the footpoints of the shorter field lines. This pattern can exist only in a 3D configuration and not in 2.5 D cylindrical geometry. It explains on its own the whirling pattern of the current density but not the unneutralized currents.

Figure 2 is a composite figure with panels of different models of twist and shear, all showing an important shear along the

PIL which is the clue to obtaining a net current. The left column concerns an emerging flux model and shows the magnetic field vectors parallel to the PIL (from Török et al. (2014)). In such a magnetic configuration there is a strong shear along the PIL. The two right columns concern the sheared field model of Dalmasse et al. (2015) with at the top right (e) for comparison the sketch by Melrose (1991) on neutralized currents with lanes of positive alternated with negative currents. This pattern is very similar, in fact, to the current density pattern (panel f) found in Dalmasse et al. (2015) for a weak shear, in which the currents are not neutralized. When the PIL is sheared the magnetic field does not have anymore a current free region around the PIL.

Dalmasse et al. (2015) concluded that magnetic shear along the PIL caused by the motions imposed in the photosphere is responsible of the unneutralized (i.e. net current) current observed in ARs and shown in current density maps. The magnetic shear generates a force-free net current. According to the different models, unneutralized currents occur when the twist/shear motions (i.e. flows) reach the PIL (Dalmasse et al. 2015). In that case, there is no way to have a potential field at the PIL, i.e. a

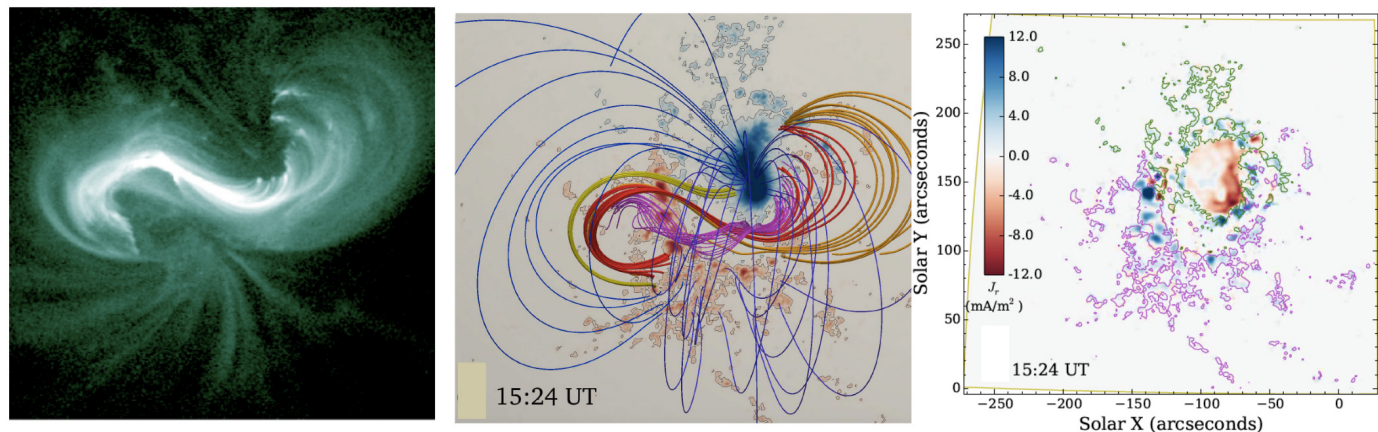


Fig. 3. Sigmoidal field lines wrapping around a flux rope in the AR 12158 which has a negative helicity (reverse S, left hand twist) on September 10, 2014, two hours before a flare. The *left panel* shows an observation in AIA 94 Å, the *middle panel* shows sigmoidal magnetic field lines using a NLFFF extrapolation based on the Grad-Rubin method (Gilchrist & Wheatland 2014), overlying a B_z map saturated at 2000 gauss and the *right panel* shows direct and return electric currents computed from HMI data after smoothing the transverse component of the observed photospheric magnetic field. The green contour outlines leading/positive magnetic field, while the purple contour outlines trailing/negative magnetic field at a field strength of ± 500 gauss. Under the force-free condition, the direct currents are red and blue in the leading positive and following negative polarity respectively according to Table 1. The return currents are blue on the right side of the main positive polarity in the green contours. The return currents (red) corresponding to the following negative polarity are more difficult to visualize (adapted from Zhao et al. (2016)).

flux rope with direct current in its core surrounded by return currents. The shear inhibits the return current along to the PIL and only direct current remains there.

In conclusion, whatever the magnetic field geometry is, the net current depends on the length of the part of the PIL above which the magnetic field is sheared, and also depends on how strong and how sheared the field is. This idea is consistent with past observations (Wheatland 2000; Falconer et al. 2002; Ravindra et al. 2011), and with the magnetic conditions found for eruptions (Falconer et al. (2002) and Guennou et al (2017)).

Several other attempts have been made to interpret the observed current density pattern. In particular Georgoulis et al. (2012) conjectured a mechanism for producing non-neutralized currents based on a dynamical compression which would generate a Lorentz force along the PIL.

2.4. Link between Coronal Structures and Photospheric Electric Currents

In addition to the question of current neutralization, another question is: can we detect flux ropes in the corona before eruptions?

In fact the observations of the corona in multi-wavelengths exhibit many structures that look like flux ropes. Many structures in the corona are considered as direct signatures of current-carrying magnetic fields such as the following:

- Forward or reversed sigmoids, bright structures with a S-shape or reverse S-shape, observed in EUV with the Atmospheric Imaging Assembly (AIA) imager aboard the *Solar Dynamical Observatory* (SDO) with the 131 Å and 94 Å filters (Gibson et al. 2006; Savcheva et al. 2012a,b), and in X-ray with Yohkoh (Canfield et al. 1999). Sigmoids are frequently inferred to be bundles of whirling field lines forming a flux rope (Dudík et al. 2014; Janvier et al. 2013; Zhao et al. 2014, 2016; Cheng et al. 2011; Cheng & Ding 2016). They are considered to be surrounding the erupting flux rope.
- The prominences, called filaments when observed on the disk, are formed by cool plasma suspended in magnetic structures with J parallel to B (Aulanier & Schmieder 2002; Mackay et al. 2010; Guo et al. 2010). Dark cavities with spinning motions observed at the limb in coronal lines (*i.e.* 193 Å and 171 Å with SDO/AIA) are also interpreted as being the signatures of flux ropes (Gibson et al. 2010; Parenti et al. 2012). They are formed by persistent shear flows and flux cancellation at PILs (van Ballegoijen & Martens 1989).

The intrinsic relationship between filaments, sigmoids and magnetic flux ropes is not obvious. It is commonly very difficult to prove that the sigmoid forms a flux rope (Zhao et al. 2016). Many studies interpret sigmoids and filaments, as indicating the presence of a flux rope because it is a direct interpretation for eruptions and coronal mass ejections. In the CME models, filaments are identified as a tracer of the flux rope, which can erupt due to the torus or breakout instabilities (Kliem & Török 2006;

Schmieder et al. 2015). Flux ropes are important because they indicate the presence of strong electric currents. Their footpoints in the photosphere should be a region with intense currents and a possible signature of their existence.

However the detection of flux ropes in the corona and their footpoints in the photosphere is not trivial. In many observations, it is not clear that the filament channel or the sigmoid plays a role in the eruption and the eruptive sigmoid can be quite different from it. For example on July 12, 2012, the filament in AR 11520 remains unperturbed during the entire flare. The flare starts in a pre-existing coronal sigmoid which does not take part of the eruption. The eruption is occurring via a second sigmoid formed by continuous slipping magnetic reconnection of the overlying arcades (Dudík et al. 2014). In this complicated case it is very difficult to define the flux rope and even more its footpoints which are moving during the entire period of the eruption. In many cases sigmoid magnetic field lines can be considered as the envelope of the flux rope. Commonly the field lines are anchored in strong magnetic field and cannot shift easily. Therefore sigmoids can be used as a proxy of a flux rope.

Nonlinear force-free field (NLFFF) extrapolations are also in principle a good tool for testing the existence of a flux rope. However the magnetic field in the boundary (photosphere) has to be modified, e.g. preprocessed which may lead to photospheric magnetic field with less free energy (Wiegelmann et al. 2010). This is the limitation of the NLFF field extrapolation studies. If the flux rope can be detected by a NLFFF extrapolation, the footpoints of the flux rope would be nevertheless better defined. We have to keep in mind that many different NLFFF methods exist and could lead to different locations of flux rope footprints. Thus the solution is also not unique.

We present in the following a case of a flux rope anchored in a sunspot with strong magnetic field ($\beta < 1$) in which case the problem of the non force-free photosphere has been somewhat avoided (Zhao et al. 2016). Figure 3 illustrates the magnetic reconstruction of the UV sigmoid observed on September 10, 2014 with AIA 94 Å using a NLFFF extrapolation based on the Grad-Rubin method (Wheatland & Gilchrist 2013; Gilchrist & Wheatland 2014; Zhao et al. 2016). One footpoint of the flux rope is surrounded by whirling bundles of extrapolated field lines anchored in the leading polarity. The second footpoint corresponds to the other end of the field bundles which is localized in the weak magnetic field negative polarity. The S shape of the sigmoid indicates that the twist of the flux rope has a negative helicity. It is a left-handed twist with currents anti-parallel to the magnetic field. The right panel in Figure 3 presents the smoothed electric current map computed from the data of HMI, the vector magnetograph on board SDO. The current density J_z in the positive leading polarity has therefore a negative sign. A ring of positive currents are well identified at the edge of this positive polarity. They correspond to the return currents. The J_z values in the negative following polarity have mainly a positive sign and represents the direct current density. The return current in that polarity is not detectable presumably because of unresolved small flux tubes of the network (following Parker, see Section 2.1).

3. ELECTRIC CURRENTS DURING ERUPTIONS

3.1. Current Ribbons

In the previous sections, we have discussed now pre-eruptive ARs are often associated with flux rope signatures. We have shown an example of direct/return currents in current density

maps in the center of an active region formed by emerging magnetic flux before an eruption. We have seen the existence of two parallel elongated current density lanes symmetrically (each ending with one hook) located on each side of the PIL (Figure 1).

Some recent studies have also started to address the properties of active currents during solar flares. Flares are characterized by a fast increase of the light emission in a wide range of the electromagnetic spectrum. During the impulsive phase the sudden increase of brightening of two elongated ribbon-like structures, which could already exist in the pre-phase as it has been shown previously is observed in visible radiation ($H\alpha$) as well as in UV wavelengths (in C IV with SMM/UVSP in Schmieder et al. (1987), in 304 Å with TRACE in Chandra et al. (2009), in different filters of AIA in Dudík et al. (2014); Janvier et al. (2014)), and sometimes in hard X-ray sources (Krucker et al. 2007; Musset et al. 2015). The two-ribbon flare models explained the bright ribbons as due to the impact in the chromosphere of the accelerated particles from the reconnection site (Forbes et al. 1989). MHD simulations obtained with the OHM code allow a 3D view of the phenomena. As described in the pre-phase of the flare, the elongated $H\alpha$ and UV brightenings coincide with the photospheric footprints of the QSLs, manifested by lanes of high current density that enclose the flux rope (Janvier et al. 2013). Reconnection occurs in current sheets in the quasi-separatrix layers (QSLs), and in particular in the thin high region underneath the flux rope. The simulations predict the increase of current density in the QSLs.

We have to point out that there are very few examples of observations of current density maps during eruptions, up to now, because it requires a rapid acquisition of the *IQUV* (Stokes parameters) in a wide region. However the time to scan an active region requires one hour, half a hour and 12 min with the THEMIS, Hinode, and HMI vector magnetographs respectively. Therefore only HMI, with its relatively high cadence, is able to follow the evolution of the current density during an eruption with a high spatial resolution. The low spectral resolution of HMI (five points along the line profile only) apparently does not strongly influence the determination of the currents because for the inversion, the code has to fit simultaneously the four Stokes parameter profiles for one pixel. So in fact it is 20 points and not five, that are fitted simultaneously. This is still a relatively small number, but it brings a lot of information. What is also important in the observations of the locations of strong current densities is the spatial continuity in the 2D maps. For isolated current concentrations that only cover one (or a few pixels), the signal could disappear in the noise.

We focus our review on the pioneering paper of Janvier et al. (2014), and on the second paper (Janvier et al. 2016) confirming the results found in the first paper for a different active region. The first paper concerns the active region AR 11158 of February 15, 2011, where a X2.1 class flare occurred. This active region was located in the northern hemisphere. This region was intensively studied (Inoue et al. 2015; Inoue 2016; Zhao et al. 2014). The region consists of the central portion of two emerging active regions which, a few days earlier, joined each other. Therefore a strong shear was developing between the two central polarities (leading and following) and led to X-class flares (Schrijver et al. 2011). The sigmoid observed in the AIA filter by SDO, not shown here, indicates the presence of a flux rope of positive helicity before the eruption.

Figure 4 focuses on the two polarities in the AR center. In the left panels are displayed the ribbons, in the middle panels, the current density J_z maps obtained from HMI. The two bright

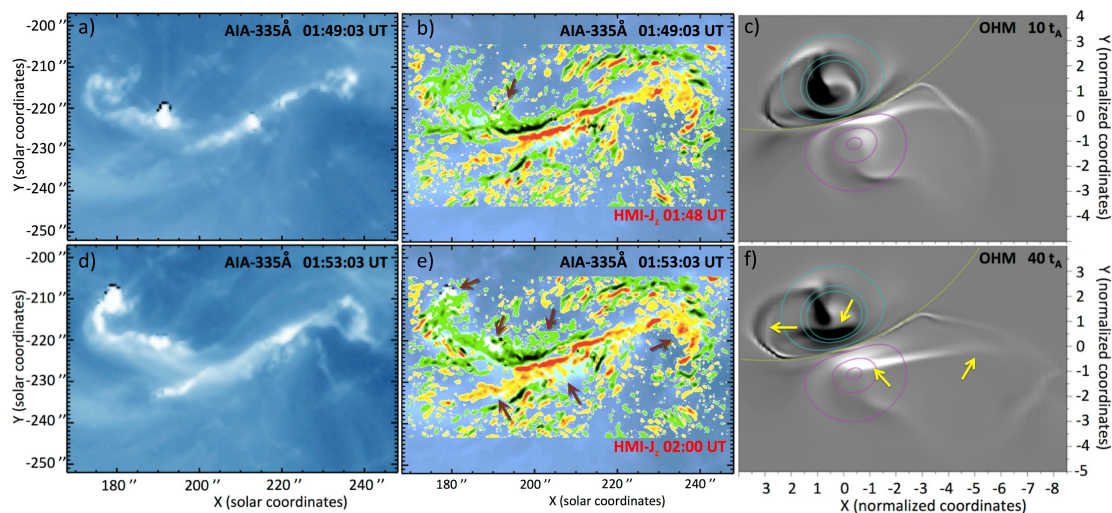


Fig. 4. (Left column): Flare ribbons at the onset (a) and during (d) the peak of the flare observed in 335 Å with SDO/AIA in AR 11158 on February 15, 2011. (Middle column): Vertical current density J_z maps (red/green are positive/negative currents saturated to $\pm 0.2 \text{ A.m}^{-2}$) from SDO/HMI before (b) and after (e) the impulsive phase superposed over a 335 Å image showing the ribbons. The flare ribbons are very well co-aligned with the current ribbons. The brown arrows show similar structures found for J_z and the ribbon maps. (Right column): J_z photospheric maps from OHM 3D simulations of an eruptive flare. The yellow arrows point out the differences seen around the end of the simulation compared to the beginning (adapted from Janvier et al. 2014).

ribbons observed in AIA 335 Å and their corresponding electric current density ribbons, J_z (negative /positive current over the negative/positive polarity) appear at the onset of the flare. The ribbons were thin and overlapped the elongated J-shaped current density lanes observed before the flare, and during the impulsive phase. They very rapidly became thicker, because the post flare loops were already developing below. The hooks became more prominent with an increase of the current density during the impulsive phase of the flare. During the eruption, the hooks increased in size. Quantitative results for the total current I integrated in the surface of boxes covering the hooks showed an increase by a factor reaching two (Janvier et al. 2014). In the second paper the increase of the total current reached an increase of 2.8 (Janvier et al. 2016).

These results have been discussed in the frame of two theoretical MHD models (Janvier et al. 2016): one using OHM (Aulanier et al. 2010) for the first paper and the other paper the model of Savcheva & van Ballegooijen (2009). Figure 4 (right panels) shows the evolution of current density maps resulting from a 3D MHD simulation of an eruptive flare (Aulanier et al. 2010; Janvier et al. 2014).

These main features are summarized in a sketch with the QSLs (grey-pink areas) and magnetic field lines (four lines) enveloping a flux rope (Figure 5). The QSLs are coronal current layers, that extend to the photosphere and are the locations of high electric current densities. The magnetic field lines are distorted at the QSLs which are a possible site of reconnection, as indicated by red arrows. The footprints of the QSLs and current layers are J-shaped (Figure 4 right panels) and the hooks surround the legs of the flux rope. The magnetic topology analysis of the February 15 2011 active region confirmed that the bright ribbons of the flare (observed in AIA/304 Å) overlaid the QSL footprints in the photosphere (see Figure 4 in Zhao et al. (2014)). The QSL footprints wrapped around the flux rope footprints in the photosphere.

The numerical simulations show that, in torus-instability models, the photospheric current ribbons can be interpreted qualitatively as the footprints of the 3D coronal current follow-

ing the QSLs (Janvier et al. 2014, 2016). The simulations being running dimensionless, no quantitative analysis has been performed on these simulations yet. As the torus instability develops, stronger electric currents are formed along the QSLs and reconnection is not fast enough to destroy them, as it is limited by the Alfvén speed (Lin et al. 2001). The first observations have confirmed that the total current increased by a factor around two during the flare.

3.2. Current Decrease at the Footpoints of the Erupting Flux Tube During and After the Eruption

As explained in the previous section, the prediction of MHD models is that the localized electric currents increase inside the flare ribbons which are the intersections of the QSLs and the photosphere (Aulanier et al. 2012). On the other hand, the MHD model predicts also that the electric current inside the flux rope should decrease due to the expansion of the flux rope (Aulanier et al. 2005). This may be deduced from flux conservation. It was demonstrated that for a cylindrical flux rope with a constant end-to-end twist, the current J_z is proportional to L^{-1} , L being its length (see equations (46) and (47) in Aulanier et al. (2005)). During the eruption the flux rope is stretched so its length increases, and the footprint currents in the photosphere should decrease. The current decreases also in catastrophic models (Forbes 2000).

However the decrease of the electric current inside the flux rope is difficult to test because of the uncertainty of the identification of the flux rope ends (see Section 2.2). However, combining two recent papers studying the same active region AR 12158 on September 10, 2014, we can conjecture that the ends of the sigmoidal loops wrapping around the flux rope found by extrapolation by Zhao et al. (2016) could correspond to the ends of the sigmoid observed in the hot channel of AIA (94 Å) and used as proxy of the flux rope ends in the Cheng & Ding (2016) paper (see Figures 3 and 6). Cheng & Ding (2016) studied the evolution of the magnetic field and the currents in two boxes contained the footprints of the sigmoid. One flux rope footprint is

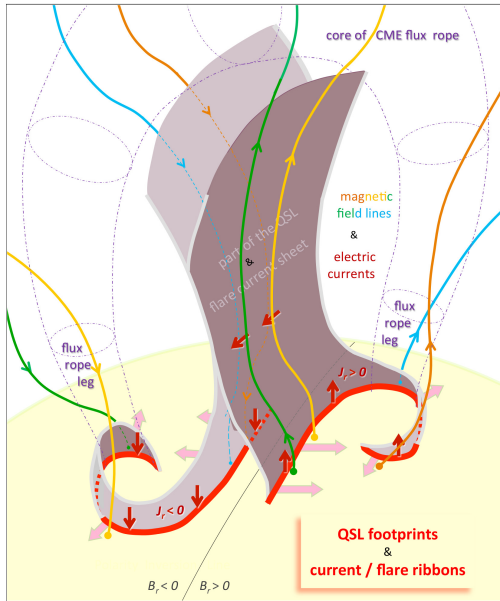


Fig. 5. Cartoon for the standard model in 3D with four pre-reconnected magnetic field lines (yellow, green). The pink-grey area represents parts of the 3D volume of the QSLs and the current layers. The red lines with hooks represent the footprints of the QSLs in the photosphere and are similar to two ribbon flares. The dashed lines with oval sections in the overlaying area of the QSLs represent the flux rope with its hook footprints in the photosphere (adapted from Janvier et al. 2014).

located in a strong field positive polarity. The second one, being in a weaker negative field corresponds to weak currents, which could be at the limit of the measurements. A decrease of the direct current is measured in the strong positive polarity (Figure 6d). These results agree with the qualitative behavior of numerical simulations which treat asymmetrical configurations, similar to the observed configuration of this AR (Aulanier et al. 2010).

The decrease of the currents is predicted by MHD models because of end-to-end twist conservation induced by line tying (Aulanier et al. 2005) and catastrophic models because of flux conservation below an erupting flux rope (Démoulin & Aulanier 2010). This is opposite to the behavior that is built in circuit models (Melrose 1991) where the total current is prescribed. Direct and quantitative comparisons between models and observations are therefore needed to better characterized the time-evolution of currents during solar flares.

4. CONCLUSION

This chapter discusses electric currents in the pre-eruption state and in the course of eruptions of solar magnetic structures, using information from solar observations, nonlinear force-free (NLFF) field extrapolations relying on these observations and three-dimensional magnetohydrodynamical (MHD) models. With the new generation of vector magnetographs new current density maps have been obtained showing in each polarity a complex whirling pattern of current density (Schmieder & Aulanier 2012).

The main topic of this chapter is to show how the new current density maps in active regions combined with the development of new 3D MHD models allows us to progressively interpret the observations and better fine-tune the understanding of MHD mechanisms, in the context of eruptions. MHD simulations of pre-eruptive active regions, based on the coronal flux rope concept, show a whirling electric current density pattern, similar to the observations in the photosphere with direct and return current in each polarity of the initial bipole (Aulanier et al. 2005, 2010; Janvier et al. 2014). The current density occurrence in bright flare ribbons in the footprints of the QSLs that separate the flux rope from the overlying arcades was an important discovery.

Before discussing eruptions, we have reported how the old problem of unneutralized currents has been resolved. The new observations of electric current density of pre-eruptive active regions have reopened the long debate on the neutralization of the currents in the "90s" by Melrose (1991) and Parker (1996a). The key parameter determining the existence of unneutralized (i.e. net current) active regions in the pre-eruptive phase has been proven to be the shear along the PIL of a bipole (Török et al. 2014; Dalmasse et al. 2015). Unneutralized photospheric current density patterns appear whenever magnetic shear is present along polarity inversion lines (which is typical of observed intense PIL, e.g. in sunspots). In the models of Dalmasse et al. (2015), shear and twist were created in the corona by artificial line-tied surface motions that were primarily aimed at building a series of differently sheared quasi force-free configurations. In reality shear could be due to the coupling of the dynamics of the emergence of a flux rope and the convection in the sub-photosphere. This shear creates the net current when the flux rope does not emerge completely. Shear along the PIL and net current are necessary for the occurrence of flares and eruptions (Falconer et al. 2002; Kliem & Török 2006).

A whirling current density pattern, observed in some active regions before eruptions, has been interpreted as the photospheric footprint of flux ropes in the corona. The currents have a hook shape which, according to the models encircles the flux rope footprint. Inside the active region two elongated current density lanes are detected, symmetrically located along the PIL when there is a strong shear before the flare. All regions do not show such a structure before the eruption but already a few cases have been published (Schmieder & Aulanier 2012; Janvier et al. 2014; Georgoulis et al. 2012). In the observed current density pattern with J-shaped hooks, the high spatial resolution allow us to distinguish the currents in the hooks and the surrounding mixed sign currents. Considering one magnetic polarity, i.e. above a sunspot, it is clear that both direct and return currents are present. The direct current is generally dominant. During the eruptions more intense current ribbons are observed and an increase of the current density in the straight part of the ribbons has been measured. The total current during an eruption in the current ribbons including their hooks has been quantified in two observational cases up to now, and shows an increase by a factor of two (Janvier et al. 2014, 2016). This can be explained qualitatively. When a flare begins, new narrow J-shaped current structures develop on top of the pre-existing relatively broad elongated current density lanes, also in J-shape. These new structures appear to match bright flare ribbons, visible from the visible to EUV wavelengths. On the contrary in regions encircled by the hooks a decrease has been detected (Cheng & Ding 2016). This can be explained by the expansion of the flux rope.

Several authors analyzed MHD simulations before and during an eruption from a qualitatively point of view (Török et al.

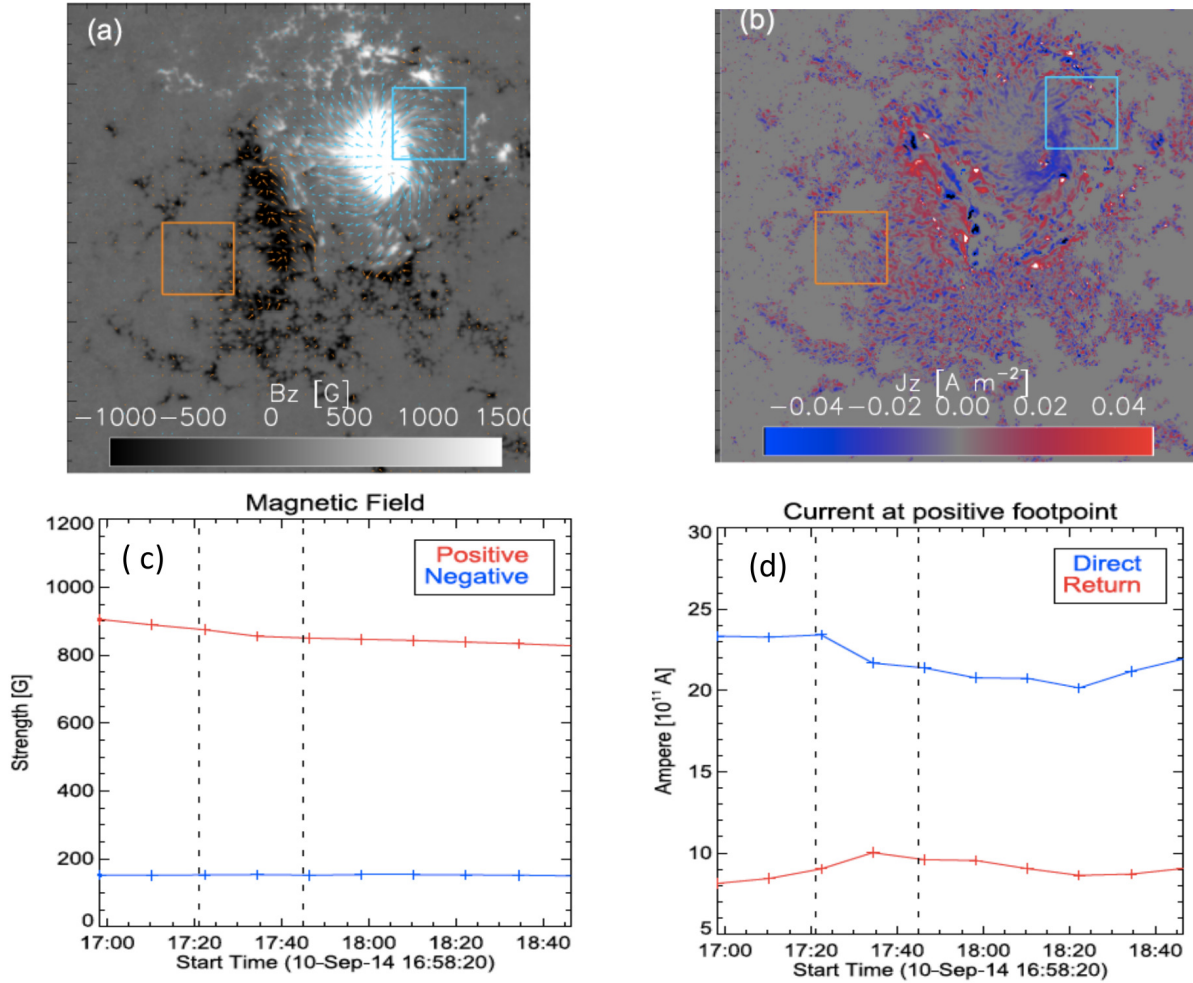


Fig. 6. Photospheric electric currents in the footpoints of the sigmoid/flux rope in AR 12158 on September 10, 2014 (the same AR as in Figure 3). (a) HMI vector magnetogram with two boxes surrounding the deduced two flux rope footpoints; (b) HMI electric current maps; (c) the mean strength of the magnetic field measured in the two boxes of panels (a) and (b); (d) the direct and return current in the positive magnetic polarity box. The two vertical lines indicate the onset and peak of the flare (adapted from Cheng & Ding (2016)).

2014; Janvier et al. 2014; Dalmasse et al. 2015). The simulations use dimensionless units and have not yet analyzed to give quantified results on the values of the current increase during an eruption, nor how much of a is decrease in the current density in the flux rope we can expect. No attempt of distinguishing direct and return current in ARs during eruptions has been carried out yet. The work still remains to be done. With the increase of computer facilities and the parallelization of codes it should be possible to estimate the net current in each polarity and to compute their variation during eruptions.

Today we have vector magnetograms with high spectral resolution (Hinode/SOT, THEMIS) in a small field of view with low time resolution. We have HMI full disk vector magnetograms with high cadence but relatively low sensitivity. In the future we may expect to have sensitive vector magnetograms with higher spatial resolution to compute electric current density with accuracy and with higher cadence to study the evolution during eruptions.

DKIST and EST (the future 4 meter telescopes) and Solar Orbiter/PHI (the Polarimetric and Helioseismic Imager), which will fly close to the Sun, will certainly bring very surprising re-

sults in this domain, on small field of views with DKIST and EST and on the full disk with PHI.

References

- Alfvén, H. & Carlqvist, P. 1967, *Sol. Phys.*, 1, 220
- Amari, T., Canou, A., & Aly, J.-J. 2014, *Nature*, 514, 465
- Amari, T., Luciani, J. F., Aly, J. J., Mikic, Z., & Linker, J. 2003a, *ApJ*, 585, 1073
- Amari, T., Luciani, J. F., Aly, J. J., Mikic, Z., & Linker, J. 2003b, *ApJ*, 595, 1231
- Archontis, V. & Török, T. 2008, *A&A*, 492, L35
- Aulanier, G., Janvier, M., & Schmieder, B. 2012, *A&A*, 543, A110
- Aulanier, G., Parlat, E., & Démoulin, P. 2005, *A&A*, 444, 961
- Aulanier, G. & Schmieder, B. 2002, *A&A*, 386, 1106
- Aulanier, G., Török, T., Démoulin, P., & DeLuca, E. E. 2010, *ApJ*, 708, 314
- Bommier, V. 2013, *Physics Research International*, Volume 2013 (2013), Article ID 195403, 16 pages, 2013
- Bommier, V., Landi Degl’Innocenti, E., Landolfi, M., & Molodij, G. 2007, *A&A*, 464, 323
- Canfield, R. C., de La Beaujardiere, J.-F., Fan, Y., et al. 1993, *ApJ*, 411, 362
- Canfield, R. C., Hudson, H. S., & McKenzie, D. E. 1999, *Geophys. Res. Lett.*, 26, 627
- Canou, A., Amari, T., Bommier, V., et al. 2009, *ApJ*, 693, L27
- Chandra, R., Schmieder, B., Aulanier, G., & Malherbe, J. M. 2009, *Sol. Phys.*, 258, 53
- Cheng, X. & Ding, M. D. 2016, *ApJS*, 225, 16
- Cheng, X., Zhang, J., Liu, Y., & Ding, M. D. 2011, *ApJ*, 732, L25

- Cheung, M. C. M. & Isobe, H. 2014, *Living Reviews in Solar Physics*, 11
- Dalmasse, K., Aulanier, G., Démoulin, P., et al. 2015, *ApJ*, 810, 17
- Démoulin, P. 2007, *Advances in Space Research*, 39, 1674
- Démoulin, P. & Aulanier, G. 2010, *ApJ*, 718, 1388
- Démoulin, P., Hénoux, J. C., Priest, E. R., & Mandrini, C. H. 1996a, *A&A*, 308, 643
- Démoulin, P. & Pariat, E. 2009, *Advances in Space Research*, 43, 1013
- Démoulin, P., Priest, E. R., & Lonie, D. P. 1996b, *J. Geophys. Res.*, 101, 7631
- Dudík, J., Janvier, M., Aulanier, G., et al. 2014, *ApJ*, 784, 144
- Falconer, D. A., Moore, R. L., & Gary, G. A. 2002, *ApJ*, 569, 1016
- Fan, Y. 2010, *ApJ*, 719, 728
- Fan, Y. & Gibson, S. E. 2003, *ApJ*, 589, L105
- Fan, Y. & Gibson, S. E. 2007, *ApJ*, 668, 1232
- Forbes, T. 2010, *Models of coronal mass ejections and flares*, ed. C. J. Schrijver & G. L. Siscoe (Cambridge University Press), 159
- Forbes, T. G. 2000, *J. Geophys. Res.*, 105, 23153
- Forbes, T. G. & Isenberg, P. A. 1991, *ApJ*, 373, 294
- Forbes, T. G., Malherbe, J. M., & Priest, E. R. 1989, *Sol. Phys.*, 120, 285
- Forbes, T. G. & Priest, E. R. 1995, *ApJ*, 446, 377
- Gary, G. A., Moore, R. L., Hagyard, M. J., & Haisch, B. M. 1987, *ApJ*, 314, 782
- Georgoulis, M. K., Titov, V. S., & Mikić, Z. 2012, *ApJ*, 761, 61
- Gibson, S. E., Fan, Y., Török, T., & Kliem, B. 2006, *Space Sci. Rev.*, 124, 131
- Gibson, S. E., Kucera, T. A., Rastawicki, D., et al. 2010, *ApJ*, 724, 1133
- Gilchrist, S. A. & Wheatland, M. S. 2014, *Sol. Phys.*, 289, 1153
- Gosain, S., Démoulin, P., & López Fuentes, M. 2014, *ApJ*, 793, 15
- Guo, Y., Ding, M. D., Schmieder, B., et al. 2010, *ApJ*, 725, L38
- Hagyard, M. J. 1988, *Sol. Phys.*, 115, 107
- Heikkilä, W. J. 1997, *J. Geophys. Res.*, 102, 9651
- Inoue, S. 2016, *Progress in Earth and Planetary Science*, 3, 19
- Inoue, S., Hayashi, K., Magara, T., Choe, G. S., & Park, Y. D. 2015, *ApJ*, 803, 73
- Javier, M., Aulanier, G., Bommier, V., et al. 2014, *ApJ*, 788, 60
- Javier, M., Aulanier, G., Pariat, E., & Démoulin, P. 2013, *A&A*, 555, A77
- Javier, M., Savcheva, A., Pariat, E., et al. 2016, *A&A*, 591, A141
- Kliem, B. & Török, T. 2006, *Physical Review Letters*, 96, 255002
- Klimchuk, J. A. & Sturrock, P. A. 1992, *ApJ*, 385, 344
- Krucker, S., White, S. M., & Lin, R. P. 2007, *ApJ*, 669, L49
- Leake, J. E., Linton, M. G., & Török, T. 2013, *ApJ*, 778, 99
- Leka, K. D., Canfield, R. C., McClymont, A. N., & van Driel-Gesztelyi, L. 1996, *ApJ*, 462, 547
- Leka, K. D. & Skumanich, A. 1999, *Sol. Phys.*, 188, 3
- Li, H., Schmieder, B., Song, M. T., & Bommier, V. 2007, *A&A*, 475, 1081
- Lin, J. & Forbes, T. G. 2000, *J. Geophys. Res.*, 105, 2375
- Lin, J., Forbes, T. G., & Isenberg, P. A. 2001, *J. Geophys. Res.*, 106, 25053
- Luoni, M. L., Démoulin, P., Mandrini, C. H., & van Driel-Gesztelyi, L. 2011, *Sol. Phys.*, 270, 45
- Mackay, D. H., Karpen, J. T., Ballester, J. L., Schmieder, B., & Aulanier, G. 2010, *Space Sci. Rev.*, 151, 333
- Martens, P. C. H. & Kuin, N. P. M. 1989, *Sol. Phys.*, 122, 263
- Melrose, D. B. 1991, *ApJ*, 381, 306
- Melrose, D. B. 1995, *ApJ*, 451, 391
- Metcalf, T. R., Leka, K. D., Barnes, G., et al. 2006, *Sol. Phys.*, 237, 267
- Molodenskii, M. M. & Filippov, B. P. 1987, *Soviet Ast.*, 31, 430
- Moreton, G. E. & Severny, A. B. 1968, *Sol. Phys.*, 3, 282
- Musset, S., Vilmer, N., & Bommier, V. 2015, *A&A*, 580, A106
- Parenti, S., Schmieder, B., Heinzl, P., & Golub, L. 2012, *ApJ*, 754, 66
- Parker, E. N. 1996a, *ApJ*, 471, 489
- Parker, E. N. 1996b, *J. Geophys. Res.*, 101, 10587
- Parker, E. N. 2001, *Ap&SS*, 277, 1
- Ravindra, B., Venkatakrishnan, P., Tiwari, S. K., & Bhattacharyya, R. 2011, *ApJ*, 740, 19
- Savcheva, A. & van Ballegoijen, A. 2009, *ApJ*, 703, 1766
- Savcheva, A. S., Green, L. M., van Ballegoijen, A. A., & DeLuca, E. E. 2012a, *ApJ*, 759, 105
- Savcheva, A. S., van Ballegoijen, A. A., & DeLuca, E. E. 2012b, *ApJ*, 744, 78
- Schmieder, B., Archontis, V., & Pariat, E. 2014, *Space Sci. Rev.*, 186, 227
- Schmieder, B. & Aulanier, G. 2012, *Advances in Space Research*, 49, 1598
- Schmieder, B., Aulanier, G., & Vršnak, B. 2015, *Sol. Phys.*, 290, 3457
- Schmieder, B., Forbes, T. G., Malherbe, J. M., & Machado, M. E. 1987, *ApJ*, 317, 956
- Schrijver, C. J., Aulanier, G., Title, A. M., Pariat, E., & Delannée, C. 2011, *ApJ*, 738, 167
- Severny, A. B. 1964, *ARA&A*, 2, 363
- Spicer, D. S. 1982, *Space Sci. Rev.*, 31, 351
- Sturrock, P. A. & Stern, R. 1980, *ApJ*, 238, 98
- Török, T. & Kliem, B. 2003, *A&A*, 406, 1043
- Török, T., Leake, J. E., Titov, V. S., et al. 2014, *ApJ*, 782, L10
- van Ballegoijen, A. A. & Martens, P. C. H. 1989, *ApJ*, 343, 971
- van Tend, W. & Kuperus, M. 1978, *Sol. Phys.*, 59, 115
- Venkatakrishnan, P. & Tiwari, S. K. 2009, *ApJ*, 706, L114
- Wheatland, M. S. 2000, *ApJ*, 532, 1209
- Wheatland, M. S. & Gilchrist, S. A. 2013, *Journal of Physics Conference Series*, 440, 012037
- Wiegmann, T., Yelles Chaouche, L., Solanki, S. K., & Lagg, A. 2010, *A&A*, 511, A4
- Wilkinson, L. K., Emslie, A. G., & Gary, G. A. 1992, *ApJ*, 392, L39
- Zhao, J., Gilchrist, S. A., Aulanier, G., et al. 2016, *ApJ*, 823, 62
- Zhao, J., Li, H., Pariat, E., et al. 2014, *ApJ*, 787, 88